Er:KY_3F_10 laser at 2.80 μm

Liza Basyrova, Pavel Loiko, Jean-Louis Doualan, Abdelmjid Benayad, Alain Braud, Christophe Labbé, Patrice Camy

To be published in Optics Letters:

Title: Er:KY3F10 laser at 2.80 µm

Authors: liza Basyrova,Pavel Loiko,Jean-Louis DOUALAN,Abdelmjid Benayad,Alain BRAUD,Christophe Labbe,Patrice Camy

Accepted: 13 October 21

Posted 14 October 21

DOI: https://doi.org/10.1364/OL.439457

Er:KY_3F_{10} laser at 2.80 µm

Liza Basyrova,[1] Pavel Loiko[1], Jean-Louis Doualan,[1] Abdelmjid Benayad,[1] Alain Braud,[1] Christophe Labbe,[1] and Patrice Camy[1,*]

[1]*Centre de Recherche sur les Ions, les Matériaux et la Photonique (CIMAP), UMR 6252 CEA-CNRS-ENSICAEN, Université de Caen Normandie, 6 Boulevard du Maréchal Juin, 14050 Caen Cedex 4, France*
**Corresponding author: patrice.camy@ensicaen.fr*

Received XX Month XXXX; revised XX Month, XXXX; accepted XX Month XXXX; posted XX Month XXXX (Doc. ID XXXXX); published XX Month XXXX

We report on the mid-infrared laser operation of a cubic 15 at.% Er^{3+}:KY_3F_{10} crystal. In the quasi-continuous-wave regime, the peak power reaches 255 mW at 2.80 µm (the $^4I_{11/2} \rightarrow {}^4I_{13/2}$ transition) with a slope efficiency of 10.9% and a laser threshold of 58 mW. Two pumping schemes (to the $^4I_{11/2}$ and $^4I_{9/2}$ states) are compared. The emission properties of Er^{3+} ions in KY_3F_{10} are studied, indicating high stimulated-emission cross-section of 0.57×10^{-20} cm² at 2.80 µm, a large gain bandwidth of 40 nm and a long $^4I_{11/2}$ state lifetime of 4.64 ms. 2021 Optical Society of America

http://dx.doi.org/10.1364/OL.99.099999

Lasers emitting at ~3 µm are of practical importance for medicine (laser surgery) [1], sensing, IR countermeasures and supercontinuum source pumping [2]. Nowadays, such emission is usually achieved in bulk and fiber lasers based on Erbium (Er^{3+}) ions owing to the $^4I_{11/2} \rightarrow {}^4I_{13/2}$ transition [3,4], Fig. 1. Due to the typically large Stark splitting of the $^4I_{13/2}$ multiplet, 2.8 µm Er lasers offer broadband wavelength tunability [5] and the option of ultrashort pulse generation [6]. They can be also easily excited at ~0.96-0.98 µm (to the upper laser level), e.g., by commercial InGaAs diode lasers [7]. Typically, the upper laser level ($^4I_{11/2}$) lifetime is shorter than the terminal level ($^4I_{13/2}$) one representing a self-terminating transition. For laser operation, this transition thus requires depletion of the lower laser level. The most efficient depletion mechanism is the energy-transfer upconversion (ETU) [8,9], $^4I_{13/2} + {}^4I_{13/2} \rightarrow {}^4I_{15/2} + {}^4I_{9/2}$, Fig. 1. Efficient ETU requires high Er^{3+} doping levels (or strong ion interactions, e.g., in clusters). The ETU can lead to laser slope efficiencies exceeding the Stokes limit due to the efficient pump energy recycling [10].

From the point of view of optimum laser host, low phonon energy materials are required to ensure weak multi-phonon non-radiative (NR) relaxation from the $^4I_{11/2}$ state. Er^{3+}-doped fluoride materials (glasses for fiber lasers [11,12] and crystals / ceramics for bulk ones) are excellent candidates for mid-IR lasers, as they provide (i) low phonon energies, (ii) low refractive indices, (iii) broadband transparency in the mid-IR and (iv) high thermal conductivity (crystals). So far, different fluoride crystals doped with Er^{3+} ions, such as cubic CaF_2 [13], SrF_2 [14] or their solid-solutions $Ca_{1-x}Sr_xF_2$ [15], tetragonal $LiYF_4$ [10] and monoclinic BaY_2F_8 [7] were implemented in mid-IR lasers. Wyss *et al.* reported on a laser-pumped 15 at.% Er^{3+}:$LiYF_4$ laser delivering ~100 mW at 2809 nm with a record-high slope efficiency of 46% and a threshold of only 42 mW [10]. By applying an InGaAs diode laser for pumping, Su *et al.* reported on power scaling of a 3 at.% Er^{3+}:SrF_2 laser to watt-level output (1.06 W at ~2.8 µm) with still high slope efficiency of 26% [14].

Potassium yttrium fluoride (KY_3F_{10}) is less common fluoride compound of the KY – YF_3 binary system. It belongs to the cubic class (sp. gr. $Fm3^-m$) and possesses a fluorite (CaF_2) type structure [16,17]. Compared to CaF_2 and its isomorphs, it has several advantages, such as lower melting temperature and the presence of a single substitutional rare-earth site [18] allowing for heavy doping. KY_3F_{10} can be grown by the conventional Czochralski (Cz) method [16]. However, it is relatively poorly studied concerning laser operation. Recently, KY_3F_{10} crystals doped with Tm^{3+} ions were revisited for efficient laser operation at ~1.9 µm [19] and ~2.3 µm [20]. For the latter laser scheme, an evidence of a strong ETU process refilling the upper laser level (a situation similar to the $^4I_{11/2} \rightarrow {}^4I_{13/2}$ Er^{3+} laser scheme) was provided [20].

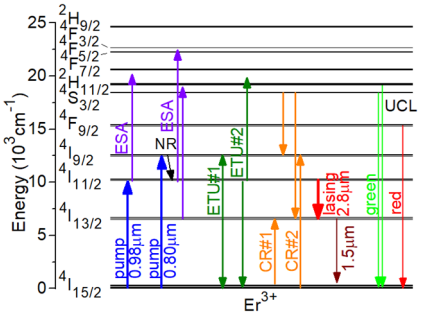

Fig. 1. Scheme of the energy levels of Er^{3+} ions in KY_3F_{10} with processes relevant for the $^4I_{11/2} \rightarrow {}^4I_{13/2}$ laser transition: pump (*blue*) and laser (*red*) transitions, ESA: excited-state absorption (*violet*), ETU: energy-transfer upconversion (*green*), CR: cross-relaxation (*orange*), UCL: upconversion luminescence.

In the present work, we aimed to revisit highly Er^{3+}-doped KY_3F_{10} crystal as a gain material for mid-IR lasers. Previously, only the spectroscopic properties of Er^{3+}:KY_3F_{10} crystals were reported [21]. In [22], the possibility of laser operation of Er^{3+}:KY_3F_{10} on the $^4F_{9/2} \rightarrow {}^4I_{9/2}$ transition at ~3.5 μm was analyzed theoretically.

KY_3F_{10} melts congruently at 1030 °C. The crystal was grown by the Cz method using a composition of 22 KY – 78 (YF_3 + ErF_3) (mol%). The nominal Er^{3+} doping level was 15 at.% and the actual doping concentration (in the crystal) N_{Er} determined by the Inductively Coupled Plasma Mass Spectrometry (ICP-MS) was 22.7×10^{20} cm^{-3} (the segregation coefficient was close to unity, ~0.98). Er^{3+}:KY_3F_{10} crystallizes in the cubic class (sp. gr. O^5_h – $Fm\bar{3}m$, No. 225) and it is optically isotropic. There is a single type if rare-earth sites (the Y^{3+} ones) having the symmetry of C_{4v} and VIII-fold fluorine coordination. Due to the closeness of ionic radii of Y^{3+} (1.16 Å) and Er^{3+} (1.14 Å) [23], high doping levels are achievable. KY_3F_{10} has a low refractive index of n = 1.47 at ~2.8 μm [21].

At first, we studied the spectral-kinetic properties relevant for the 2.8 μm laser. The stimulated-emission (SE) cross-sections, σ_{SE}, for the $^4I_{11/2} \rightarrow {}^4I_{13/2}$ transition were calculated by the Fuchtbauer–Ladenburg equation using the luminescence spectrum measured in the present work and the radiative lifetime τ_{rad} of 6.14 ms and the luminescence branching ratio $\beta_{JJ'}$ of 15.8% taken from [21], Fig. 2(a). The maximum σ_{SE} is 1.77×10^{-20} cm^2 at 2730 nm, corresponding to the zero-phonon line (ZPL) transition, Fig. 2(a).

For the excited-state absorption (ESA) process from the terminal laser level, $^4I_{13/2} \rightarrow {}^4I_{11/2}$, the cross-sections, σ_{ESA}, were calculated by means of the reciprocity method, Fig. 2(a), using the crystal-field splitting for Er^{3+} in KY_3F_{10} [21]. The maximum σ_{ESA} of 1.64×10^{-20} cm^2 corresponds to the zero-phonon-line (ZPL) transition at 2730 nm, i.e., the transition between the lowest Stark sub-levels of the two multiplets.

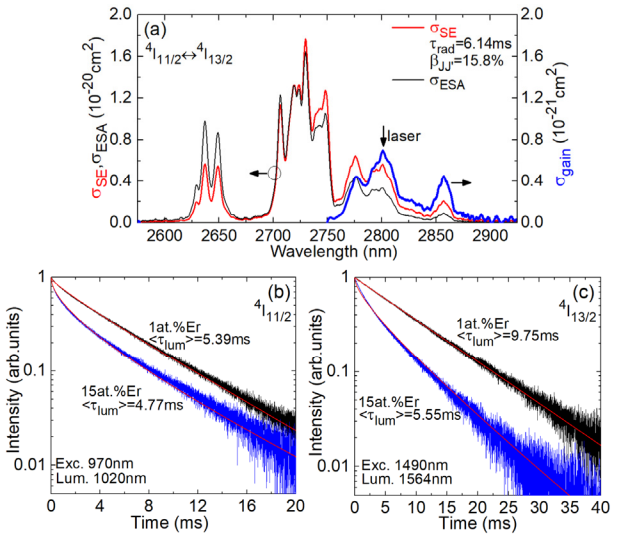

Fig. 2. Emission properties of Er^{3+}:KY_3F_{10}: (a) stimulated-emission (SE, *red*), σ_{SE}, excited-state absorption (ESA, *black*), σ_{ESA}, and gain (*blue*), σ_{gain}, cross-sections for the $^4I_{11/2} \leftrightarrow {}^4I_{13/2}$ transitions, the *arrow* indicates the laser wavelength, the inversion ratio β = 0.45; (b,c) luminescence decay curves from (b) the $^4I_{11/2}$ state and (c) the $^4I_{13/2}$ state for 1 and 15 at.% Er doping, *red curves* – fitting using the I-H model [24], <τ_{lum}> - mean luminescence lifetime.

The luminescence decay curves from the $^4I_{11/2}$ and $^4I_{13/2}$ states of Er^{3+} in KY_3F_{10} are shown in Fig. 2(b,c), measured using immersed powders to avoid the radiation trapping effect. The measured decay curves from both states are clearly not single exponential owing to the strong ETU. They are reasonably good fitted using the Inokuti-Hirayama (I-H) model [24] assuming dipole-dipole interactions. In addition, average luminescence lifetimes were calculated as $\langle\tau_{lum}\rangle = \int I(t)tdt/\int I(t)dt$. For 1 at.% Er, they are 5.39 ms ($^4I_{11/2}$) and 9.75 ms ($^4I_{13/2}$). By increasing the doping level up to 15 at.% Er, the upper-state and lower-state lifetimes are reduced to 4.77 ms ($^4I_{11/2}$) and 5.55 ms ($^4I_{13/2}$), respectively, representing a more favorable ratio for 2.8 μm laser operation.

For laser experiments, a cylindrical element (diameter: 5.0 mm, thickness: 2.2 mm) was cut from 15 at.% Er^{3+}:KY_3F_{10}. Both its faces were polished to laser-grade quality and remained uncoated. The crystal was mounted on a passively cooled Cu-holder using silver paint.

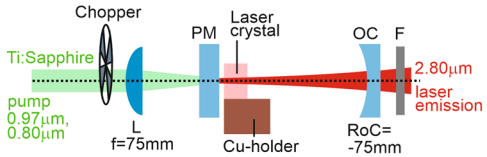

Fig. 3. Scheme of the Er^{3+}:KY_3F_{10} laser: L – focusing lens, PM – pump mirror, OC – output coupler, F – long-pass filter.

The scheme of the laser is shown in Fig. 3. The hemispherical cavity was formed by a flat pump mirror (PM) coated for high transmission at 0.78-0.83 μm (T > 97%) and 0.92-1.06 μm (T > 85%) (the pump ranges) and for high reflection (HR, R > 99.9%) at 2.6-3.0 μm and a concave output coupler (OC) having a radius of curvature (RoC) of -75 mm and a transmission T_{OC} of 1.5% at ~2.8 μm. As KY_3F_{10} provides a negative thermal lens [19], it cannot be used in a microchip cavity. The crystal was placed near the PM with an airgap ~100 μm. The cavity length was ~74 mm. As a pump source, we used a CW Ti:Sapphire laser delivering up to 3 W at 0.75 – 1.05 μm in the fundamental mode ($M^2 \approx 1$). The pump radiation was focused into the crystal using a B-coated achromatic lens with a focal length f = 75 mm. The measured pump spot radius at the $1/e^2$ level w_P was 33±5 μm. The pump absorption was determined from pump-transmission measurements under non-lasing conditions at the threshold pump powers accounting for the Fresnel losses at the uncoated crystal and second pump pass (the OC was partially reflective for the pump, e.g., $R \approx 10\%$ at 0.97 μm). The resulting values (η_{abs} = 92.8% at 0.97 μm) were slightly smaller than the small-signal ones representing ground-state bleaching. The pump was modulated using a mechanical chopper (25 Hz, duty cycles: 1:2 to 1:4, pump pulse duration: ~20 ms) for quasi-CW operation. A long-pass filter was used to filter out the non-absorbed pump. The laser emission spectra were measured using a Fourier transform laser spectrum analyzer. The laser mode in the far-field was captured using a pyroelectric camera.

At first, we studied pumping directly into the $^4I_{11/2}$ multiplet (the upper laser level) and selected the most intense absorption peak at 970.6 nm. In the quasi-CW regime with a duty cycle of 1:4, the laser generated a maximum peak output power of 255 mW at 2.80 μm with a slope efficiency η of 10.9% (versus the absorbed pump power) and a laser threshold P_{th} of 58 mW, as shown in Fig. 4(a).

The optical-to-optical efficiency η_{opt} was 9.7% (vs. the pump power incident in the crystal P_{inc}). Further power scaling was limited by the available pump and no thermal roll-over nor crystal fracture were observed until the maximum P_{inc} of 2.60 W. When reducing the duty cycle in the quasi-CW regime (down to 1:3 and 1:2), a thermal roll-over was observed. Thus, for the true CW operation, the pump power was limited to 0.72 W to avoid the risk of thermal fracture of the passively cooled crystal. The CW output power reached 57 mW, as shown in Fig. 4(a).

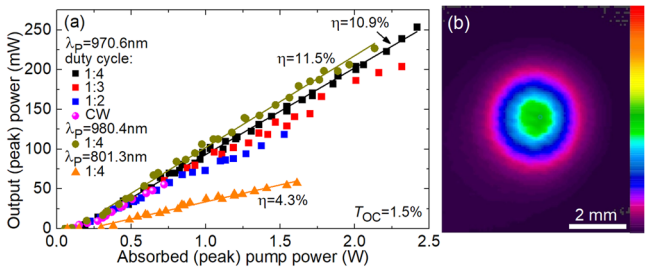

Fig. 4. Mid-infrared Er^{3+}:KY_3F_{10} laser: (a) input-output dependences, η – slope efficiency, λ_P – pump wavelength, T_{OC} = 1.5%; (b) far-field mode profile, duty cycle 1:4, P_{abs} ~1.0 W, λ_P = 970.6 nm. CW – continuous-wave operation.

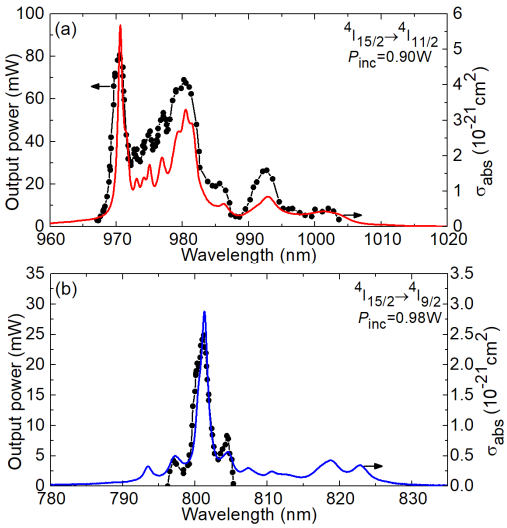

Fig. 5. Laser excitation curves for the mid-infrared Er^{3+}:KY_3F_{10} laser for pumping: (a) into the $^4I_{11/2}$ state, (b) into the $^4I_{9/2}$ state. The absorption cross-section, σ_{abs}, spectra are shown for comparison. Duty cycle: 1:4.

For the $^4I_{15/2} \rightarrow {}^4I_{11/2}$ pump transition, the laser excitation curve (the dependence of the output power on the pump wavelength λ_P at fixed P_{inc}) was measured, see Fig. 5(a). It was compared with the corresponding GSA cross-section, σ_{abs}, spectrum. It was possible to achieve lasing for λ_P in the range of 967 – 1004 nm. The highest output power corresponded to the most intense absorption peak with $\sigma_{abs} = 0.57\times10^{-20}$ cm^2 at 970.6 nm and a small bandwidth (full width at half maximum, FWHM) of 1.0 nm. Much broader peak is observed at longer wavelengths, with $\sigma_{abs} = 0.33\times10^{-20}$ cm^2 at 980.4 nm and FWHM = 4.1 nm. Pumping into this peak provided slightly better laser efficiency: the laser generated 228 mW at 2.80 μm with η = 11.5% and P_{th} = 55 mW (in the quasi-CW regime with a duty cycle of 1:4), see Fig. 4(a). This was probably due to the more uniform pump distribution in the crystal. The peak at 980.4 nm looks suitable for the use of InGaAs diode lasers as pump sources as it is expected to provide weaker sensitivity to the temperature drift of the pump wavelength.

Another possible pump transition is the $^4I_{15/2} \rightarrow {}^4I_{9/2}$ one and it is interesting for the use of AlGaAs diode lasers. The $^4I_{9/2}$ state of Er^{3+} ions in KY_3F_{10} is short-living (lifetime: ~5 μs) and the ions relax fast to the lower-lying $^4I_{11/2}$ upper laser level via multi-phonon non-radiative (NR) relaxation, Fig. 1. By pumping into the most intense absorption peak at 801.3 nm, the laser generated 58 mW at 2.80 μm with smaller η = 4.3% and higher P_{th} = 71 mW (as compared to pumping into the $^4I_{11/2}$ state) in the quasi-CW regime with a duty cycle of 1:4. The deterioration of the laser performance originates mainly from the lower Stokes efficiency and stronger heat loading for this pump scheme. The laser excitation curve for pumping into the $^4I_{9/2}$ state was also measured, Fig. 5(b). The laser operation was achieved in much narrower range of λ_P, 796 - 805 nm. The main absorption peak of Er^{3+} ions is also relatively narrow with σ_{abs} = 0.29×10^{-20} cm^2 at 801.3 nm and FWHM = 1.6 nm, Fig. 5(b).

The Er^{3+}:KY_3F_{10} laser operated at the fundamental transverse mode (measured M^2_{xy} < 1.2) with a nearly circular far-field mode profile, Fig. 4(b).

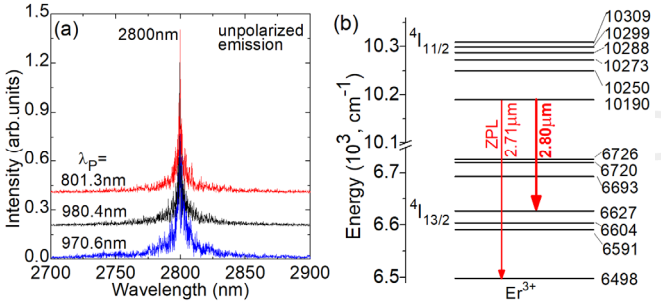

Fig. 6. (a) Typical emission spectra of the Er^{3+}:KY_3F_{10} laser; (b) crystal-field splitting of the $^4I_{11/2}$ and $^4I_{13/2}$ multiplets of Er^{3+} ions in C_{4v} sites in KY_3F_{10}, *numbers* – Stark energies in cm^{-1}, ZPL – zero-phonon line, *bold red arrow* – laser transition.

The typical spectra of laser emission are shown in Fig. 6(a). They are nearly independent on λ_P; the laser wavelength is centered at 2800 nm. It is longer than the main peak in the SE cross-section spectrum at 2730 nm. This behavior is due to the ESA process $^4I_{13/2} \rightarrow {}^4I_{11/2}$, Fig. 2(a), leading to reabsorption at the laser wavelength. The population of the terminal laser level ($^4I_{13/2}$) can be relatively high due to its long lifetime, so that the ESA from this level can be significant. Thus, the gain cross-sections, $\sigma_{gain} = \beta\sigma_{SE} - (1-\beta)\sigma_{ESA}$, are calculated to conclude about the laser wavelength. Here, β is the inversion ratio, $\beta = N_3/(N_2 + N_3)$, N_3 and N_2 are the $^4I_{11/2}$ and $^4I_{13/2}$ state populations, respectively. According to the previous gain studies, for pump power densities similar to those applied in the present work, the inversion ratio β in highly doped Er^{3+}:KY_3F_{10} can be about 0.45 [21]. The gain spectrum, Fig. 2(a), presents a local maximum at 2800 nm (in agreement with the laser wavelength) and a gain bandwidth (FWHM) of ~40 nm. The laser wavelength was assigned to an electronic transition between the Stark sub-

levels with the energies 10190 cm^{-1} ($^4I_{11/2}$) and 6627 cm^{-1} ($^4I_{13/2}$), Fig. 6(b).

Typical oscilloscope traces of the pump (at 970.6 nm) and laser (at 2800 nm) radiation for the Er^{3+}:KY_3F_{10} laser are shown in Fig. 7. After switching on the pump, relaxation oscillations are observed within ~1 ms followed by a stable CW output. Without a chopper, true CW operation occurs. The weak slow intensity instabilities for the laser radiation originate from the pump instabilities.

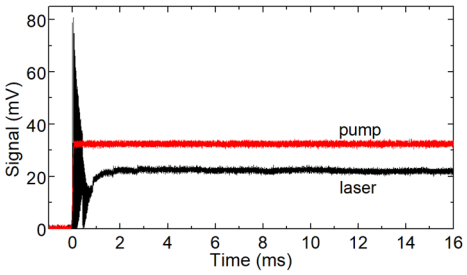

Fig. 7. Oscilloscope traces of the pump (0.97 μm) and laser (2.8 μm) radiation from the Er^{3+}:KY_3F_{10} laser.

The round-trip passive losses were estimated using a simple model of a quasi-four-level laser [25], $L = 3.3\pm0.5\%$. For the correct description of the laser threshold, it was essential to consider the reabsorption loss due to the ESA, $\sigma_{ESA} = 0.34\times10^{-20}$ cm^2 at 2.80 μm.

The Er^{3+}:KY_3F_{10} crystal under optical pumping exhibited yellow-green upconversion luminescence (UCL) originating from the $^4S_{3/2} + {}^2H_{11/2} \rightarrow {}^4I_{15/2}$ (at 546 nm) and $^4F_{9/2} \rightarrow {}^4I_{15/2}$ (at 667 nm) transitions. Considering the high Er^{3+} doping level, the corresponding excited states are mainly populated by the ETU #2 process, Fig. 1.

To conclude, we report on the first laser operation of a highly Er^{3+} doped cubic potassium yttrium fluoride (KY_3F_{10}) crystal in the mid-IR spectral range. Two pump schemes (pumping into the $^4I_{11/2}$ and $^4I_{9/2}$ states) were implemented. The quasi-CW Er^{3+}:KY_3F_{10} laser generated up to 255 mW at 2.80 μm with a slope efficiency up to 11.5% and a laser threshold down to 55 mW. The true CW laser operation without any pulsed instabilities was realized as well. The power scaling in the CW regime was limited by thermal effects in the passively cooled crystal. Excited-state absorption from the terminal level ($^4I_{13/2}$) plays an important role in establishing the laser wavelength being longer than the ZPL; the emission is assigned to a single Stark transition. We believe that further improvement of the laser efficiency is possible by (i) reducing the passive losses in the crystal under optimized growth conditions (a proper control of the pulling rate and evaporation of KF changing the melt stoichiometry) and (ii) optimizing the Er^{3+} concentration between 7 – 15 at.%. The latter is crucial for finding a proper ratio between the rate constants of the two ETU processes depleting the $^4I_{13/2}$ and $^4I_{11/2}$ states, Fig. 1. Further power scaling is expected by a proper thermal management of the laser crystal, e.g., by applying active cooling, as well as the use of ~980 nm InGaAs diode lasers as pump sources. The effect of Er doping in the thermal conductivity should be also revealed. Er^{3+}:KY_3F_{10} crystals also provide relatively large gain bandwidth around ~2.8 μm which is attractive for ultrashort pulse generation.

Funding. French Agence Nationale de la Recherche (ANR), SPLENDID2 (ANR-19-CE08-0028).

Disclosures. The authors declare no conflicts of interest.

Data availability. Data underlying the results presented in this paper are not publicly available at this time but may be obtained from the authors upon reasonable request.

References

1. T. Harashima, J. I. Kinoshita, Y. Kimura, A. Brugnera, F. Zanin, J.D. Pecora, and K. Matsumoto, Photomed. Laser Surg. **23**, 52 (2005).
2. 2. T. S. Saini, N. P. Trung Hoa, K. Nagasaka, X. Luo, T. H. Tuan, T. Suzuki, and Y. Ohishi, Appl. Opt. **57**, 1689 (2018).
3. R. C. Stoneman and L. Esterowitz, Opt. Lett. **17**, 816-818 (1992).
4. T. Jensen, A. Diening, G. Huber, and B. H. T. Chai, Opt. Lett. **21**, 585 (1996).
5. J. Šulc, M. Němec, R. Švejkar, H. Jelínková, M. E. Doroshenko, P. P. Fedorov, and V. V. Osiko, Opt. Lett. **38**, 3406 (2013).
6. P. Tang, Z. Qin, J. Liu, C. Zhao, G. Xie, S. Wen, and L. Qian, Opt. Lett. **40**, 4855-4858 (2015).
7. M. Pollnau, W. Lüthy, H. P. Weber, T. Jensen, G. Huber, A. Cassanho, H. P. Jenssen, and R. A. McFarlane, Opt. Lett. **21**, 48 (1996).
8. M. Pollnau, T. Graf, J. E. Balmer, W. Lüthy, and H. P. Weber, Phys. Rev. A. **49**, 3990 (1994).
9. S. Tokita, M. Murakami, S. Shimizu, M. Hashida, and S. Sakabe, Opt. Lett. **34**, 3062 (2009).
10. C. Wyss, W. Lüthy, H. P. Weber, P. Rogin, and J. Hulliger, Opt. Commun. **139**, 215 (1997).
11. D. Faucher, M. Bernier, G. Androz, N. Caron, and R. Vallée, Opt. Lett. **36**, 1104 (2011).
12. X. Zhu and R. Jain, Opt. Lett. **32**, 2381 (2007).
13. C. Labbe, J. L. Doualan, P. Camy, R. Moncorgé, and M. Thuau, Opt. Commun. **209**,193 (2002).
14. L. Su, X. Guo, D. Jiang, Q. Wu, Z. Qin, and G. Xie, Opt. Express **26**, 5558 (2018).
15. Z. Zhang, F. Ma, X. Guo, J. Wang, X. Qian, J. Liu, J. Liu, and L. Su, Opt. Mater. Express **8**, 3820 (2018).
16. M. Diaf, A. Braud, C. Labbé, J. L. Doualan, S. Girard, J. Margerie, R. Moncorgé, and M. Thuau, Can. J. Phys. **77**, 693 (2000).
17. M. Schellhorn, D.Parisi, S. Veronesi, G. Bolognesi, M. Eichhorn, and M.Tonelli, Opt. Lett. **38**, 504 (2013).
18. K. Friese, H. Krüger, V. Kahlenberg, T. Balić-Zunić, H. Emerich, J. Y. Gesland, and A. Grzechnik, J. Phys. Condens. Matter **18**, 2677 (2006).
19. M. Chen, P. Loiko, J. M. Serres, S. Veronesi, M. Tonelli, M. Aguiló, F. Díaz, S. Y. Choi, J. E. Bae, F. Rotermund, S. Dai, Z. Chen, U. Griebner, V. Petrov, and X. Mateos, J. Alloy Compd **813**, 152176-1 (2020).
20. L. Guillemot, P. Loiko, R. Soulard, A. Braud, J. L. Doualan, A. Hideur, and P. Camy, Opt. Express **28**, 3451 (2020).
21. C. Labbé, J. L. Doualan, R. Moncorgé, A. Braud, and P. Camy, Opt. Mater. **79**, 279 (2018).
22. S. Luo, R. Moncorgé, J.-L. Doualan, H. Xu, Z. Cai, C. Labbé, B. Xu, A. Braud, and P. Camy, J. Opt. Soc. Am. B **36**, 275 (2019).
23. A. A. Kaminskii, *Crystalline Lasers: Physical Processes and Operating Schemes* (CRC Press, 1996).
24. M. Inokuti, F. Hirayama, J. Chem. Phys. **43**, 1978 (1965).
25. J. M. Serres, V. Jambunathan, P. Loiko, X. Mateos, H. Yu, H. Zhang, J. Liu, A. Lucianetti, T. Mocek, K. Yumashev, U. Griebner, V. Petrov, M. Aguiló, and F. Díaz, Opt. Mater. Express **6**, 46 (2016).

Full references

1. T. Harashima, J. I. Kinoshita, Y. Kimura, A. Brugnera, F. Zanin, J.D. Pecora, and K. Matsumoto, "Morphological comparative study on ablation of dental hard tissues at cavity preparation by Er:YAG and Er,Cr:YSGG lasers, " Photomed. Laser Surg. **23**(1), 52-55 (2005).
2. T. S. Saini, N. P. Trung Hoa, K. Nagasaka, X. Luo, T. H.Tuan, T. Suzuki, and Y. Ohishi, "Coherent midinfrared supercontinuum generation using a rib waveguide pumped with 200 fs laser pulses at 2.8 μm," Appl. Opt. **57**(7), 1689-1693 (2018).
3. R. C. Stoneman and L. Esterowitz, "Efficient resonantly pumped 2.8-μm Er^{3+}:GSGG laser," Opt. Lett. **17**(11), 816-818 (1992).
4. T. Jensen, A. Diening, G. Huber, and B. H. T. Chai, "Investigation of diode-pumped 2.8-μm Er:$LiYF_4$ lasers with various doping levels," Opt. Lett. **21**(8), 585-587 (1996).
5. J. Šulc, M. Němec, R. Švejkar, H. Jelínková, M. E. Doroshenko, P. P. Fedorov, and V. V. Osiko, "Diode-pumped Er:CaF_2 ceramic 2.7 μm tunable laser," Opt. Lett. **38**(17), pp.3406-3409 (2013).
6. P. Tang, Z. Qin, J. Liu, C. Zhao, G. Xie, S. Wen, and L. Qian, "Watt-level passively mode-locked Er^{3+}-doped ZBLAN fiber laser at 2.8 μm," Opt. Lett. **40**(21), 4855-4858 (2015).
7. M. Pollnau, W. Lüthy, H. P. Weber, T. Jensen, G. Huber, A. Cassanho, H. P. Jenssen, and R. A. McFarlane, "Investigation of diode-pumped 2.8-μm laser performance in Er:BaY_2F_8," Opt. Lett. **21**(1), 48-50 (1996).
8. M. Pollnau, T. Graf, J. E. Balmer, W. Lüthy, and H. P. Weber, Explanation of the cw operation of the Er^{3+} 3-μm crystal laser, Phys. Rev. A. **49**(5), 3990-3996 (1994).
9. S. Tokita, M. Murakami, S. Shimizu, M. Hashida, and S. Sakabe, "Liquid-cooled 24 W mid-infrared Er:ZBLAN fiber laser," Opt. Lett. **34**(20), 3062-3064 (2009).
10. C. Wyss, W. Lüthy, H. P. Weber, P. Rogin, and J. Hulliger, "Emission properties of an optimised 2.8 μm Er^{3+}:YLF laser," Opt. Commun. **139**(4-6), 215-218 (1997).
11. D. Faucher, M. Bernier, G. Androz, N. Caron, and R. Vallée, "20 W passively cooled single-mode all-fiber laser at 2.8 μm," Opt. Lett. **36**(7), 1104-1106 (2011).
12. X. Zhu and R. Jain, "Compact 2 W wavelength-tunable Er:ZBLAN mid-infrared fiber laser," Opt. Lett. **32**(16), 2381-2383 (2007).
13. C. Labbe, J. L. Doualan, P. Camy, R. Moncorgé, and M. Thuau, "The 2.8μm laser properties of Er^{3+} doped CaF_2 crystals," Opt. Commun. **209**(1-3), 193-199 (2002).
14. L. Su, X. Guo, D. Jiang, Q. Wu, Z. Qin, and G. Xie, "Highly-efficient mid-infrared CW laser operation in a lightly-doped 3 at.% Er:SrF_2 single crystal," Opt. Express **26**(5), 5558-5563 (2018).
15. Z. Zhang, F. Ma, X. Guo, J. Wang, X. Qian, J. Liu, J. Liu, and L. Su, "Mid-infrared spectral properties and laser performance of Er^{3+} doped $Ca_xSr_{1-x}F_2$ single crystals," Opt. Mater. Express **8**(12), 3820-3828 (2018).
16. M. Diaf, A. Braud, C. Labbé, J. L. Doualan, S. Girard, J. Margerie, R. Moncorgé, and M. Thuau. "Synthesis and spectroscopic studies of Tm^{3+}-doped KY_3F_{10} single crystals, " Can. J. Phys. **77**(9), 693-697 (2000)
17. M. Schellhorn, D.Parisi, S. Veronesi, G. Bolognesi, M. Eichhorn, and M.Tonelli, "In-band pumped Ho^{3+}:KY_3F_{10} 2 μm laser," Opt. Lett. **38**(4), 504-506 (2013).
18. K. Friese, H. Krüger, V. Kahlenberg, T. Balić-Zunić, H. Emerich, J. Y. Gesland, and A. Grzechnik, "Study of the temperature dependence of the structure of KY_3F_{10}," J. Phys. Condens. Matter **18**(9), 2677-2687 (2006).
19. M. Chen, P. Loiko, J. M. Serres, S. Veronesi, M. Tonelli, M. Aguiló, F. Díaz, S. Y. Choi, J. E. Bae, F. Rotermund, S. Dai, Z. Chen, U. Griebner, V. Petrov, and X. Mateos, "Fluorite-type Tm^{3+}:KY_3F_{10}: A promising crystal for watt-level lasers at ~1.9 μm," J. Alloy Compd **813**, 152176-1-8 (2020).
20. L.Guillemot, P. Loiko, R. Soulard, A. Braud, J. L. Doualan, A. Hideur, and P. Camy, "Close look on cubic Tm:KY_3F_{10} crystal for highly efficient lasing on the $^3H_4 \rightarrow {}^3H_5$ transition," Opt. Express **28**(3), 3451-3463 (2020).
21. C. Labbé, J. L. Doualan, R. Moncorgé, A. Braud, and P. Camy, "Excited-state absorption and fluorescence dynamics of Er^{3+}:KY_3F_{10}," Opt. Mater. **79**, 279-288 (2018).
22. S. Luo, R. Moncorgé, J.-L. Doualan, H. Xu, Z. Cai, C. Labbé, B. Xu, A. Braud, and P. Camy, "Simulation of dual-wavelength pumped 3.5 μm CW laser operation of Er:CaF_2 and Er:KY_3F_{10} in waveguide configuration," J. Opt. Soc. Am. B **36**(2), 275-284 (2019).
23. A. A. Kaminskii, *Crystalline Lasers: Physical Processes and Operating Schemes* (CRC Press, 1996).
24. M. Inokuti, F. Hirayama, "Influence of energy transfer by the exchange mechanism on donor luminescence," J. Chem. Phys. **43**(6), 1978-1989 (1965).
25. J. M. Serres, V. Jambunathan, P. Loiko, X. Mateos, H. Yu, H. Zhang, J. Liu, A. Lucianetti, T. Mocek, K. Yumashev, U. Griebner, V. Petrov, M. Aguiló, and F. Díaz, "Microchip laser operation of Yb-doped gallium garnets," Opt. Mater. Express **6**(1), 46-57 (2016).